Thermal-spike treatment of ion-induced grain growth: Theory and experimental comparison

Dale E. Alexander
Materials Science Division, Argonne National Laboratory, 9700 South Cass Avenue, Argonne, Illinois 60439

Gary S. Was
Department of Nuclear Engineering, University of Michigan, Ann Arbor, Michigan 48109
(Received 7 October 1991; revised manuscript received 2 July 1992)

Grain growth commonly observed during heavy-ion irradiation of initially fine-grained (≤ 100 Å diameter) thin films is modeled as a thermal-spike phenomenon in which temperature spikes caused by ions and recoils induce atomic jumps across grain boundaries, promoting boundary migration. In elemental and homogeneous alloy systems, in which grain growth is driven solely by the reduction of boundary surface area, the model predicts that the ion-induced grain-boundary mobility is linearly proportional to the quantity, $F_D^2/\Delta H_{\rm coh}^3$, in which F_D is the ion and recoil energy deposited in elastic collisions and $\Delta H_{\rm coh}$ is the cohesive energy of the target. The model was evaluated with respect to data from two previously published ion-induced grain-growth experiments on elemental and coevaporated alloy films. The results were consistent with the thermal-spike model. Combining analytical results of the model with the experimental data it was possible to determine the value of the proportionality constant β relating the cohesive energy to the activation energy Q for grain growth ($Q=-\beta\Delta H_{\rm coh}$). The value of β for the coevaporated and elemental films, respectively, was 0.07 and 0.15, which is less than or about equal to the value previously determined for the thermal-spike treatment of ion beam mixing ($\beta_{\rm IM}=0.14$). The smaller value of β determined for the coevaporated films is consistent with the idea that atom migration across grain boundaries is easier than migration within the lattice. The thermal-spike treatment was also applied to ion-induced grain growth in multilayer films. The presence of concentration gradients in these systems adds another driving force affecting grain growth. In addition, the influence of the heat of mixing ($\Delta H_{\rm mix}$) on atomic mobility and boundary migration was incorporated in the model via a Darken effect.

I. INTRODUCTION

Ion irradiation has been observed to induce nearly athermal grain growth in thin polycrystalline metal, semiconductor, and multilayer films.[1–14] An example of this process is illustrated in Fig. 1, which shows the effect of 1.7 MeV Xe ion irradiation on the microstructure of a 400 Å thick Pt-Ti multilayer film irradiated at room temperature.[1] The grain size is observed to increase from the as-deposited average size of <100 Å to an average size of 1080 Å, well in excess of the film thickness, after an ion dose of 1×10^{16} cm^{-2}.

The results shown in Fig. 1 are consistent with a number of investigations using bombarding ions ranging in mass from light (e.g., N) to heavy (e.g., Xe) and with ion energies ranging from a few tens of keV to a few MeV. Irradiation is capable of inducing grain growth even at low temperatures (e.g., liquid-nitrogen temperature) where thermally activated processes are normally absent. Grain size L is characteristically observed to increase monotonically with ion dose Φ typically showing a power dependence of the form $L\propto\Phi^{1/n}$ with n varying such that $1.0\leq n\leq4.5$. The uniformity of ion-induced grain growth combined with the dose dependence on grain size (or time dependence for a constant dose rate) are analogous to grain-growth behavior observed in isothermal annealing experiments. This suggests that the same driving force is operative in both. The driving force most typically associated with normal thermally-induced grain

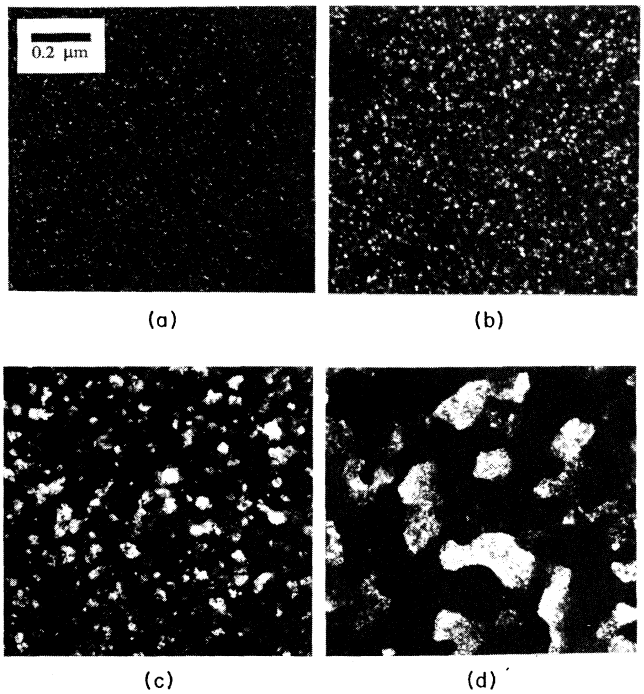

FIG. 1. Example of ion-induced grain growth in Pt-Ti multilayer films irradiated with 1.7 MeV Xe ions at room temperature. (a) As-deposited, (b) 10^{14} cm^{-2}, (c) 10^{15} cm^{-2}, (d) 10^{16} cm^{-2}.

growth is the system energy reduction resulting from the decrease in grain boundary surface area.

The study of ion-induced grain growth is of interest for a couple of reasons. The ability to control grain size athermally in thin films using such a technique has significant practical implications. For example in micorelectronics, grain size is an important factor that determines the electromigrative characteristics of thin-film devices. The ability to increase grain size using ion irradiation can avoid detrimental effects associated with interdiffusion and phase formation that may accompany thermal processing. In addition to such practical implications, the study of ion-induced grain growth should provide further insight into the fundamental nature of ion-solid interactions.

In this paper, following a review of existing models of ion-induced grain growth, a model is presented that incorporates the irradiation effect concept of thermal spikes. This model is then evaluated with respect to previous experimental data from irradiated single phase and multilayer films in order to evaluate its validity.

II. BACKGROUND

The importance of ion-induced grain-growth phenomenon, as described above, has led to a number of studies performed over the past 10 years. Systematic irradiation experiments have been conducted to examine the effect of ion mass, ion energy, dose, dose rate, temperature, and material properties on ion-induced grain growth. In spite of these studies, a complete understanding of the phenomena is still lacking. An important goal of these experiments has been to correlate the damage effects of irradiation with the observations of ion-induced grain growth. In attempting such, it is instructive to briefly review the displacement processes that occur during ion irradiation.[15–18]

When an energetic ion penetrates a crystalline solid, displacements of lattice atoms can occur as a result of elastic collisions. These displaced atoms, or recoils, in turn cause further displacements. The resulting cascade develops very quickly, on the order of 10^{-13} sec, and this collisional phase of the cascade ends when the recoil atoms or ion no longer possess sufficient kinetic energy to cause further displacements in the lattice. The interactions in the collisional phase are accurately described by a series of binary collision interactions. The initial phase is followed by a relaxation phase, again on the order of 10^{-13} sec, in which a fraction of displaced atoms and vacancies can recombine. Finally, the kinetic energy of the remaining recoiling atoms is thermalized within the lattice. The mean free path between ion or recoil interactions with lattice atoms is on the order of the interatomic spacing. Interactions are no longer adequately described by binary collisions but rather are many body in nature. This latter phase, lasting on the order of 10^{-11} sec, is termed the "thermal-spike" phase and further short-range atomic motion may be induced by thermal agitation within the local volume of the spike.

As outlined above, irradiation damage may result from atomic displacements induced during both the binary collision phase and the thermal-spike phase. One of the important questions that emerge in understanding ion-induced grain growth, is the relative importance of each of these phases to the grain-boundary migration process. In the displacement or collisional phase, the important parameters determining defect production are the mass and the atomic number of the ion and target along with the target density and the displacement energy. The Monte Carlo program TRIM[19] models the interactions in the displacement phase and can be used to calculate the energy deposited in elastic collisions, F_D. A certain fraction of this energy goes into producing N_d Frenkel defects per incident ion. Unlike the high-energy collisional phase, the average kinetic energy during the thermal spike phase is low (≤ 1 eV) and hence atom migration and defect production is strongly affected by material related thermochemical quantities (e.g., cohesive energy, ΔH_{coh}), which are of a similar magnitude. The many-bodied nature of interactions in this phase precludes a simple determination of defect production as is possible in the displacement phase. The complexity requires either molecular-dynamic simulations or the use of simplifying assumptions in order to address the situation analytically.

Previously, Atwater, Thompson, and Smith[7,20] suggested that the ion-induced grain-growth process is collisional in nature and proposed a transition-state model in which defects produced on or near grain boundaries contribute to grain-boundary migration. Grain growth is modeled as a bimolecular process consisting of vacant site formation on one side of a grain boundary followed by atom migration across the boundary to the vacant site. Two possible scenarios are conceived. The first involves vacant site formation induced by ion bombardment followed by thermally-induced atom migration to the vacant site. The second involves a collision-induced interstitial migrating to a collision-induced vacant site. In either case, the resulting analysis predicts that the ion-induced grain-boundary mobility M_{ion} should be proportional to the defect generation rate. Alternatively, since a linear dependence exists between the defects produced per ion with the energy deposited in elastic collisions, the Atwater relationship may be expressed as a first-order dependence on F_D,

$$M_{\text{ion}} = C_1 F_D \ , \tag{1}$$

where C_1 is a constant.

While the Atwater, Thompson, and Smith model is successful in describing observations in irradiated Si, Ge, and Au films,[7] more recent experiments suggest that displacement phenomena alone are inadequate for describing ion-induced grain growth. For example, Li, Liu, and Mayer[2] observed large differences in grain growth among irradiated Pt and Au films, despite the fact that their similar masses and displacement energies suggested that they should have the same collisional behavior (same F_D). Liu,[21] Liu and Mayer[12] and Alexander, Was, and Rehn[1] observed variations in grain-growth rates that scaled with the cohesive energy, ΔH_{coh}, of the targets, indicating that

material parameters, in addition to collisional related material properties, are also important.

These observations led Liu[21] and Liu, Li and Mayer[5] to suggest that ion-induced grain growth is a thermal-spike phenomenon. As described above, during the thermal-spike phase of a cascade, the remaining kinetic energy of the recoils is thermalized in the lattice. This results in the formation of temperature spikes in small localized regions of the lattice. If the spikes occur on or near a grain boundary, atoms can be thermally activated to jump across the boundary. If a net number of atoms jumps occur in one direction, the boundary migrates in the opposite direction.

Liu[21] proposed that the ion-induced grain-boundary mobility in the temperature-independent regime is proportional to a thermal-spike parameter relating the number of atom jumps induced per unit length by a thermal spike. Using Vineyard's analysis,[22] the mobility may therefore be expressed as,

$$M_{\text{ion}} = C_2 \frac{F_D^2}{\Delta H_{\text{coh}}^2} , \tag{2}$$

where C_2 is a constant. Hence the thermal-spike approach predicts a different dependence on F_D than the displacement model of Atwater, Thompson, and Smith [Eq. (1)]. Furthermore, it is noted that the nature of the target is incorporated by the presence of the cohesive energy term in Eq. (2).

The proposed thermal-spike approach of Liu, offers considerable potential for describing the ion-induced grain-growth phenomenon. This is particularly true for heavy-ion irradiation in which atomic transport, for example during ion-beam mixing, has been previously shown to be dominated by such spike effects.[24] However, the correlation of the grain-boundary mobility with thermal-spike effects, represented by Eq. (2), results essentially from qualitative arguments. This is in contrast to the more extensive theoretical treatment of the displacement model presented in Ref. 7. In this paper, a complete treatment of thermal-spike grain-growth theory is provided. In addition to grain growth in homogeneous, single phase films, the model is developed to describe ion-induced grain growth in multilayer systems. Following the model development, the results are evaluated with respect to data from previous experiments.

III. Thermal-Spike Model Development

Derivation of the model requires relating the atomistic displacement effects of thermal spikes with measurable macroscopic quantities of grain growth. To this end, an atomistic model of grain-boundary migration is used. The velocity dL/dt of an isolated boundary in one dimension can be described by,[23]

$$\frac{dL}{dt} = -M \frac{\partial \mu}{\partial x} , \tag{3}$$

where M is defined as the grain-boundary mobility, and the gradient in the chemical potential $\partial \mu / \partial x$ is the driving force associated with the boundary motion. For normal grain growth, migration is assumed to occur by thermally activated atom jumps across a boundary. The driving force for this process is proportional to the grain-boundary curvature, the reduction of which results in an overall decrease in grain-boundary area. As illustrated in Fig. 2, due to the radius of curvature in the boundary, a free-energy difference exists across the boundary. Under conditions of thermal agitation, the atoms of grain I will be activated to jump across the boundary to an available vacant site at the boundary of grain II. In doing so, a finite free-energy decrease, $\Delta \mu$, is realized. As atoms jump from grain I to grain II, the boundary moves in toward its center of curvature.

The thermal-spike approach proposes that the heat cylindrical spikes produced during heavy-ion irradiation induce the atom jumps across grain boundaries. In order to apply thermal-spike concepts, it is necessary to derive a parameter η defined as the number of atom jumps across a grain boundary induced per unit length of spike per spike. With this parameter, macroscopic grain growth can then be related by the following argument assuming that one ion produces one thermal spike at each

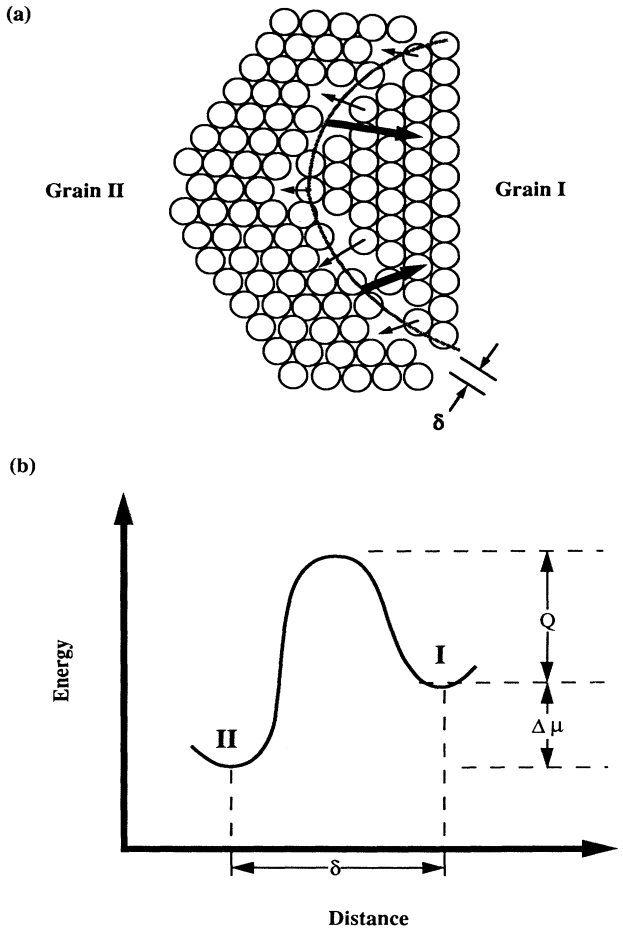

FIG. 2. (a) Schematic of atomistic grain-growth process. (b) Free energy across the boundary pictured in (a). δ, grain-boundary width, Q, activation energy for grain growth; $\Delta \mu$, chemical-potential difference across the grain boundary.

grain boundary through which the ion passes. After a dose, Φ, of ions the total number of jumps induced by thermal spikes per unit volume of material is $\eta\Phi$. The total number of jumps per atom is $\eta\Phi/\rho$, where ρ is the atomic density. In the vicinity of a grain boundary, these atom jumps, when biased preferentially in one direction, displace the boundary by a distance δ, where δ is equal to the boundary width. After an increment of dose $\Delta\Phi$, the distance a grain boundary migrates is $\Delta L=\eta\delta\Delta\Phi/\rho$. Therefore, presuming a constant ion dose rate $\dot{\Phi}$, the grain-growth rate is expressed as

$$\frac{dL}{dt}=\frac{\eta\delta\dot{\Phi}}{\rho} . \tag{4}$$

Thus, Eq. (4) relates the irradiation effects of thermal spikes (η) with macroscopic grain growth. The key therefore is to derive the parameter η and this will be done following the analytical treatment of Vineyard.[22]

A cylindrical thermal spike is assumed to be induced from the energy deposited by an ion or recoil penetrating a crystalline lattice. The ion or recoil instantaneously deposits energy in the lattice at a constant specified linear energy loss, F_D, (energy per unit length deposited in elastic collisions) and the subsequent dissipation of this energy results in the creation of a temperature distribution in a small localized cylindrical volume. An analytical expression for the temperature distribution $T(s,t)$ resulting from the energy deposition can be obtained by solving the heat conduction equation, in cylindrical geometry, considering at time $t=0$ an initial distribution of deposited energy as $F_D\delta^2(s)$ where $\delta^2(s)$ is the two-dimensional delta function with s the radial distance from the cylinder axis. Vineyard solved this equation by assuming a simple power-law dependence for the thermal conductivity κ and heat capacity c on temperature such that $\kappa=\kappa_0 T^{p-1}$ and $c=c_0 T^{p-1}$ ($p\geq 1$). The solution obtained was[22]

$$T(s,t)=\left[\frac{pF_D}{4\pi\kappa_0 t}\right]^{1/p} e^{-c_0 s^2/4p\kappa_0 t} , \tag{5}$$

where t is the time, κ_0 and c_0 are the ambient values of the thermal conductivity and the heat capacity, respectively.

Vineyard[22] used the temperature distribution given in Eq. (5) to determine η for the case in which atomic jumps in a material have a directionally random, Arrhenius behavior of the form,

$$R_{\text{rand}}=Ae^{-Q/kT} , \tag{6}$$

where R_{rand} is the atomic jump rate per unit volume, Q is the activation energy for jumping, k is Boltzmann's constant, and A is a constant independent of temperature. Under these conditions, η_{rand} is found by substituting $T=T(s,t)$ from Eq. (5) into Eq. (6) and integrating the resulting expression over the volume and duration of the spike:

$$\eta_{\text{rand}}=\int_0^\infty 2\pi s\, ds \int_0^\infty R_{\text{rand}}(s,t)dt . \tag{7}$$

This integration is simplified by a change of variables[22] and the solution using the temperature distribution given in Eq. (5) is

$$\eta_{\text{rand}}=\frac{AF_D^2 p^3}{8\pi\kappa_0 c_0}\left[\frac{k}{Q}\right]^{2p}\Gamma(2p) , \tag{8}$$

where $\Gamma(2p)$ is the gamma function with argument $2p$.

Vineyard's result [Eq. (8)] was based on the assumption of *random* atomic migration. However, as discussed earlier, atom migration in the vicinity of a curved grain boundary is biased and, therefore, a more generalized form of the atom jump rate density, $R(s,t)$, must be derived, which accounts for the presence of a biasing driving force.

Using the reaction rate arguments,[23] $R=R(s,t)$, in the presence of a biasing driving force, is first obtained for a steady-state, uniform temperature typical of an isothermal annealing experiment. Figure 2(b) illustrates the free energy for atoms located at different sites labeled I and II. Site II is at a slightly lower free energy than site I and as a result, a potential gradient exists, which may be approximated by $\Delta\mu/\delta$. Under conditions of thermal agitation at a constant temperature T, there will be a net transfer of atoms from I to II as a result of the potential gradient and the net transfer rate ν_{net} is

$$\nu_{\text{net}}=k_0 e^{-Q/kT}(1-e^{-\Delta\mu/kT}) , \tag{9}$$

where k_0 is a frequency factor. This rate expression is independent of the origin of the chemical-potential difference, $\Delta\mu$. Equation (9) is further simplified by assuming that $\Delta\mu \ll kT$. This is a valid assumption for the present work, since the average kinetic energy typically associated with atoms in thermal spikes is estimated at $kT\approx 1$ eV.[24] Typical boundary curvature driving forces are on the order $\Delta\mu<0.05$ eV for grain sizes <100 Å. Using this assumption, the exponential term in parentheses may be approximated by a series expansion and after multiplying by the atomic density ρ, the atom jump rate density R is

$$R=\frac{k_0\rho\Delta\mu}{kT}e^{-Q/kT} . \tag{10}$$

The general procedure will now be to substitute the appropriate expression for $\Delta\mu$ due to a specific driving force into Eq. (10) and then determine η by integrating over volume and duration of the spike. The resulting expression for η will thus include the effect of the driving force on atom migration within the thermal spike. η is then related to macroscopic grain-boundary migration through Eq. (4). In the discussion that follows, two driving forces are of particular interest: grain-boundary curvature and concentration gradients.

A. The effect of a grain-boundary curvature chemical-potential gradient

Normal grain growth in single phase systems is believed to be driven by the reduction in grain-boundary surface area or conversely, the reduction in grain-boundary curvature. The effect of this driving force on ion-induced grain growth is now determined by deriving η.

The chemical-potential difference resulting from boundary curvature is given by the Gibbs-Thompson expression,

$$\Delta\mu = \frac{-4\gamma\Omega}{L} , \tag{11}$$

where γ is the surface energy, Ω is the atomic volume, and L is the average grain diameter (or size). Substituting this into Eq. (10) yields the net rate per unit volume of atom migration across a curved boundary in a material characterized by a uniform temperature T,

$$R = \frac{4k_0\gamma\Omega\rho}{kTL} e^{-Q/kT} . \tag{12}$$

The expression for η is then obtained by substituting the temperature distribution given by Eq. (5) into Eq. (12) and integrating over the volume and duration of the spike,

$$\eta = \int_0^\infty 2\pi s\, ds \int_0^\infty \frac{4k_0\gamma\Omega\rho}{kL} \frac{e^{-Q/kT(s,t)}}{T(s,t)} dt . \tag{13}$$

For the purpose of determining η, the grain size L is assumed to be constant during the very short ($\sim 10^{-11}$ sec) lifetime of the thermal spike. Using a change of variables,[22] the integration yields,

$$\eta = \frac{k_0\gamma\Omega\rho k^2 F_D^2}{\pi\kappa_0 c_0 L Q^3} , \tag{14}$$

where p, the exponent used to scale the temperature dependence of the thermal conductivity and heat capacity, has been set equal to 1 for lack of a better understanding of the temperature environment within a thermal spike.

Equation (14) is further modified by assuming that the activation energy scales with the cohesive energy according to,[25]

$$Q = -\beta\Delta H_{\text{coh}} , \tag{15}$$

where β is a positive constant, η becomes

$$\eta = -\frac{k_0\gamma\Omega\rho k^2}{\pi\kappa_0 c_0 L\beta^3} \frac{F_D^2}{\Delta H_{\text{coh}}^3} . \tag{16}$$

This expression for η is different from that used previously by Liu in the description of ion-induced grain growth [see Eq. (2)]. Liu assumed η proportional to $F_D^2/\Delta H_{\text{coh}}^2$ whereas the more complete derivation given above shows that η is proportional to $F_D^2/\Delta H_{\text{coh}}^3$.

The grain-growth rate is determined by substituting Eq. (16) into Eq. (4),

$$\frac{dL}{dt} = -\frac{k_0\gamma\Omega\delta\dot{\Phi}k^2}{\pi\kappa_0 c_0\beta^3} \frac{F_D^2}{\Delta H_{\text{coh}}^3} \frac{1}{L} . \tag{17}$$

The ion-induced grain-boundary mobility, M_{ion}, may be found by rewriting Eq. (17) in the form of Eq. (3). Using Eq. (11) for the gradient term, M_{ion} becomes

$$M_{\text{ion}} = -\frac{k_0\delta^2 k^2\dot{\Phi}}{4\pi\kappa_0 c_0\beta^3} \frac{F_D^2}{\Delta H_{\text{coh}}^3} . \tag{18}$$

Since $\Delta H_{\text{coh}} < 0$ the ion-induced mobility $M_{\text{ion}} > 0$.

B. The combined effect of curvature and concentration chemical-potential gradients

Grain growth is also a common observation during ion-beam mixing of multilayers.[1] In addition to the effect of a boundary curvature chemical-potential gradient, concentration gradients in these films can affect boundary migration. A Darken effect[26] may be present that enhances or inhibits atomic migration in the concentration gradient hence affecting the mobility of boundaries located within the gradient. This effect on atomic mobility has been previously used to model interdiffusion during ion-beam mixing.[24] In that approach, variations in the intermixing rates are observed to correlate with the magnitude and sign of the thermochemical quantity, the heat of mixing (ΔH_{mix}). A similar approach may be used here to address the effect of concentration gradients on grain growth, which in turn can be used to determine the combined effect of the two driving forces on boundary migration during irradiation.

The one-dimensional nature of the concentration gradients in multilayer films (i.e., parallel to the film normal) restricts the effect of the concentration driving force to only those boundaries with a component of migration parallel to the gradient. Figure 3(a) illustrates a geometry for which the effect of this driving force is most pro-

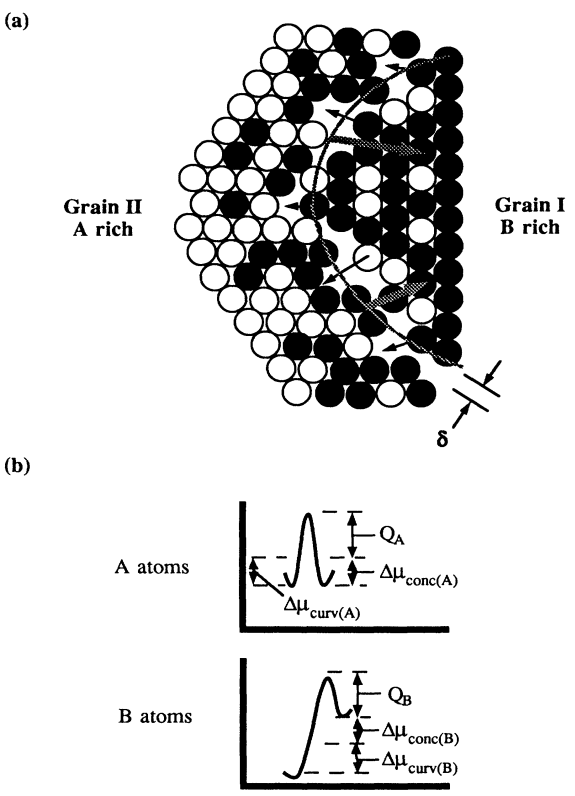

FIG. 3. (a) Schematic of atomistic grain-growth process in the presence of a concentration gradient. (b) Free energy of A and B atoms across the grain boundary pictured in (a).

nounced; the direction of boundary curvature and the concentration gradients are parallel. The grain-boundary migration rate is defined as positive when the boundary moves to the right toward the B component. The direction of the boundary curvature with respect to the concentration gradient however is not arbitrary. In order for the concentration effect to occur as modeled here there must be a specific orientation relationship. If the direction is random, no net effect due to concentration gradients would be observed on grain growth.

Using the one-dimensional geometry as defined in Fig. 3(a), the presence of concentration gradients give rise to chemical-potential gradients in addition to those associated with boundary curvature. In the case of a regular solution, the chemical-potential difference across the grain boundary of the ith component is approximated by,[23,24]

$$\Delta\mu_i = kT\left[1-\frac{2\Delta H_{\mathrm{mix}}}{kT}\right]\frac{\Delta\rho_i}{\rho_i}\ , \tag{19}$$

where ΔH_{mix} is the heat of mixing, and $\Delta\rho_i$ is the change in the atomic concentration across the grain boundary of the ith component.

Using the Gibbs-Thompson chemical-potential difference [Eq. (11)] combined with that given in Eq. (19), it is possible to derive the total thermal-spike parameter η_{TOT} that is the sum of the combined effects of concentration (η_{conc}) and boundary curvature (η') gradients [Eqs. (A13)–(A15)],

$$\eta_{\mathrm{conc}} = \frac{k_0\rho k^2 F_D^2}{\pi\kappa_0 c_0\beta^2}\left[\frac{\Delta\rho_B}{\rho_B}\frac{f_B}{8\Delta H^2_{\mathrm{coh}(B)}}\left[1+\frac{4}{\beta}-\frac{\Delta H_{\mathrm{mix}}}{\Delta H_{\mathrm{coh}(B)}}\right]-\frac{\Delta\rho_A}{\rho_A}\frac{f_A}{8\Delta H^2_{\mathrm{coh}(A)}}\left[1+\frac{4}{\beta}\frac{\Delta H_{\mathrm{mix}}}{\Delta H_{\mathrm{coh}(A)}}\right]\right], \tag{20}$$

$$\eta' = -\frac{k_0\gamma\Omega\rho k^2 F_D^2}{\pi\kappa_0 c_0 L\beta^3}\left[\frac{f_A}{\Delta H^3_{\mathrm{coh}(A)}}+\frac{f_B}{\Delta H^3_{\mathrm{coh}(B)}}\right]. \tag{21}$$

$$\eta_{\mathrm{tot}} = \frac{k_0\rho k^2 F_D^2}{\pi\kappa_0 c_0\beta^2}\left[\frac{\Delta\rho_B}{\rho_B}\frac{f_B}{8\Delta H^2_{\mathrm{coh}(B)}}\left[1+\frac{4}{\beta}\frac{\Delta H_{\mathrm{mix}}}{\Delta H_{\mathrm{coh}(B)}}\right]-\frac{\Delta\rho_A}{\rho_A}\frac{f_A}{8\Delta H^2_{\mathrm{coh}(A)}}\left[1+\frac{4}{\beta}\frac{\Delta H_{\mathrm{mix}}}{\Delta H_{\mathrm{coh}(A)}}\right]-\frac{\gamma\Omega}{\beta L}\left[\frac{f_A}{\Delta H^3_{\mathrm{coh}(A)}}+\frac{f_B}{\Delta H^3_{\mathrm{coh}(B)}}\right]\right], \tag{22}$$

where the subscripts A,B denote the binary atomic components of the multilayer film. $f_{A,B}$ are the atom fractions of components A and B, respectively.

The expression for η_{TOT} given by Eq. (22) is substituted in Eq. (4) to obtain the one-dimensional equation of motion for a grain boundary in a concentration gradient. Unlike the previous case for which the sole driving force was grain-boundary curvature, the position and time dependence of η_{TOT} (as determined by the concentration terms ρ_i, $\Delta\rho_i$) precludes a simple analytical derivation of an ion-induced mobility. Instead, an iterative approach is required to analyze the grain-growth rate of an isolated boundary coupled with the solution of the diffusion equation to determine the proper form of the concentration gradient. A complete analysis is thus more complex and involves an interplay between ion mixing (interdiffusion, changes in the concentration gradient) and boundary migration (position in the concentration gradient).

It is observed from Eq. (22), when the cohesive energies of the two components are equal, the concentration gradient contribution [Eq. (20)] of η_{TOT} cancels out and the result reduces essentially to that obtained previously for the sole driving force due to boundary curvature [Eq. (18)]. Since the activation energies for diffusion scale with the cohesive energies (i.e., $Q=-\beta\Delta H_{\mathrm{coh}}$), this result indicates that no *net* flux of atoms diffuse across the boundary. As modeled, concentration gradients will affect grain growth only if there is a net flux of atoms across the boundary as a result of unequal activation energies for diffusion.

IV. MODEL APPLICATION TO EXPERIMENTAL RESULTS

A. Single phase, elemental, and coevaporated films

The thermal-spike model developed for the sole effect of boundary curvature predicts a linear dependence of the ion-induced grain-boundary mobility on the parameter $F_D^2/\Delta H^3_{\mathrm{coh}}$ [see Eq. (18)]. This dependence can be evaluated with respect to experimental grain-growth data obtained previously for single phase, elemental, and coevaporated alloy films. Table I lists experiments performed on films of this type in which grain size L was measured as a function of ion dose Φ for a variety of ion/target combinations.

A fundamental difficulty encountered in comparing results from the experiments listed in Table I is the differences in grain-size measurement techniques applied. The variety of techniques used results from the difficulty in applying standard grain-size measurement techniques (e.g., intercept methods) to irradiated thin-film microstructures. Tests of linearity predicted by Eq. (18) must therefore be restricted to data from a specific experiment rather than attempting to interpret the data from all experiments collectively.

Two criteria were addressed in selecting experiments from Table I for analysis. First, only those experiments involving heavy ions were examined, since these were expected to produce the cylindrical thermal-spike effects modeled. Second, of those remaining only those consist-

TABLE I. Summary of ion/target combinations used in previous systematic ion-induced grain-growth experiments of single phase metallic films.

Film (−at. %)	Ion	Energy (keV)	Reference
Pt-15 Ti	Xe	1700	1
Pt-15 V	Xe	1700	1
Ni-23 Al	Xe	1700	1
Pt-17 Ni	Xe	1700	1
Au-10 Co	Xe	1700	1
Au	Ar	200	2
Pt	Ar	200	2
Ni	Xe	560	3
Ni	Kr	310	3
Ni	Ar	240	3
Pd	Xe	560	4
Pd	Ar	185	4
Pd	Ne	100	4
Cu	Ar	200	5
Co	Xe	600	6
Ni	Xe	600	6
V	Xe	600	6
Cr	Xe	600	6
Ti	Xe	600	6
Au	Xe	200	7
Au	Kr	200	7
Ni	Bi	100–200	10
Ni	Ag	40–130	10,11
Ni	P	a	13
Au	N	80	14
Ag	N	80	14
Cu	N	80	14

[a]Ion energy not indicated in reference.

ing of greater than two ion/target combinations were considered. This latter criteria was necessary because, as described above, the linearity predicted by the thermal-spike model must be tested within a given experimental data set, requiring more than two data points. These criteria are satisfied by the experiments performed in Refs. 1, 6, 10, and 11 (see Table I). However, the lower ion energies used in the experiments involving Ag- and Bi-irradiated Ni films[10,11] resulted in substantial incorporation of the irradiating species in the films. This alloying was expected to significantly affect mobility and therefore these experiments were not analyzed. Thus the Xe-irradiated coevaporated films of Ref. 1 and the Xe-irradiated elemental films of Ref. 6 were chosen for analysis.

Evaluation of the model required determining F_D and ΔH_{coh} values for the various ion energy/target combinations and also deriving values of M_{ion} from the experimental grain-growth data. Since the experiments described in Ref. 6 did not contain dose-rate information, it was necessary to use a dose-rate-normalized mobility quantity, $M_{\text{ion}}/\dot{\Phi}$, instead of simply M_{ion}. Values of F_D were obtained from TRIM v.5.5 calculations[19] in which 1000 histories were run under full cascade conditions with displacement energies set equal to 25 eV and binding energies set equal to 2 eV. The F_D values quoted in Table II represent the total ion and recoil energy deposited in elastic collisions. Values for cohesive energy found in Table II were taken from Ref. 27.

Experimentally derived values of the normalized mobility, $M_{\text{ion}}/\dot{\Phi}$, were obtained using the following procedure. Grain size L versus ion dose Φ data was fit according to the expression,

$$L^n - L_0^n = K\Phi \ , \tag{23}$$

with L_0 the measured initial grain size, n the best-fit growth exponent, and K a best-fit constant. This expression is analogous to that used to describe the kinetics of isothermal normal grain growth with time t replacing ion dose Φ. The data was fit over the entire dose range examined in the experiments: $0-3\times10^{15}$ cm^{-2} for the coevaporated films[1] and $0-7.5\times10^{15}$ cm^{-2} for the elemental films.[6] The resulting fit parameters for the experiments are found in Table II. Equation (23) was then differentiated with respect to Φ to obtain an expression for $dL/d\Phi$,

TABLE II. Parameters used in analysis of ion-induced grain-growth experimental data from single phase films.

Film	Energy		ΔH_{coh}	F_D	$L^n-L_0^n=K\Phi$ Fit parameters K		$\frac{F_D^2}{\Delta H_{\text{coh}}^3}$	$\frac{M_{\text{ion}}}{\dot{\Phi}}$	
(−at %)	(keV)-Ion	Ref.	(eV)	(eV/Å)	(Å^{n}cm^2)	n	$\left[\frac{1}{\text{Å}^2\text{eV}}\right]$	$\left[\times10^6\frac{\text{Å}^4}{\text{eV}}\right]$	β
Pt-15 Ti	1700-Xe	1	6.21	425	9.66×10^{-10}	2.4	754	0.88	0.07
Pt-15 V	1700-Xe	1	6.04	415	1.11×10^{-8}	2.8	785	1.56	
Ni-23 Al	1700-Xe	1	4.43	355	1.61×10^{-8}	3.2	1450	0.46	
Pt-17 Ni	1700-Xe	1	5.63	455	1.62×10^{-8}	2.8	1160	1.78	
Au-10 Co	1700-Xe	1	3.83	400	8.55×10^{-6}	3.6	2847	5.24	
Co	600-Xe	6	4.39	455	3.04×10^{-5}	4.5	2447	0.57	0.15
Ni	600-Xe	6	4.44	485	1.40×10^{-9}	2.8	2687	0.19	
V	600-Xe	6	5.31	324	8.35×10^{-7}	4.2	701	0.18	
Cr	600-Xe	6	4.10	382	1.43×10^{-8}	3.5	2117	0.12	
Ti	600-Xe	6	4.85	230	3.74×10^{-8}	3.8	464	0.08	

$$\frac{dL}{d\Phi}=\frac{K}{n}(K\Phi+L_0^n)^{(1/n)-1} . \quad (24)$$

Using the fit parameters, the normalized mobility was then found from the slope of $dL/d\Phi$ values versus $\partial\mu/\partial x=-4\gamma\Omega/\delta L$ values evaluated over a range of ion dose. For this portion of the analysis, doses were restricted such that $\Phi\geq 10^{14}$ cm^{-2} in order to avoid contributing data from very small grain sizes. The spike-activated grain-growth process, as described above, is not likely to provide a valid description for the very small grain-size regime in which the dimensions of disorder induced by thermal spikes are greater than or equal to the size of the grains.

It is notable that when $n=2$, Eq. (23) is the integrated result of Eq. (3) using the Gibbs-Thompson driving force. However, the growth exponent n has been experimentally observed to vary in the range from $1.0\leq n\leq 4.5$. In the analogous case of thermal grain growth, it has been shown that $n>2$ can result if an inhibiting driving force independent of grain size is present.[28] In such a case, Eq. (3) is simply modified by the addition of a constant term opposing the Gibbs-Thompson driving force. The above analysis used to extract the normalized boundary mobility is independent of such constant and therefore remains valid.

Figure 4 shows the results of the analysis, as applied to the two sets of experimental data. Least-squared linear fits were determined for each experiment excluding the Ni-Al and Ni data from the coevaporated and elemental data sets respectively. In the Ni-Al samples,[1] irradiation induced the formation of a hexagonal close-packed (HCP) phase in addition to the face-centered-cubic phase. Although not explicitly detailed in Ref. 6, elemental Ni[3] was also previously observed to transform to HCP during heavy-ion irradiation. The presence of two phases may have lowered grain-boundary mobility in these samples and therefore they were excluded from the linear fits.

Examination of the thermal-spike analysis results shown in Fig. 4 support the linearity predicted by Eq.

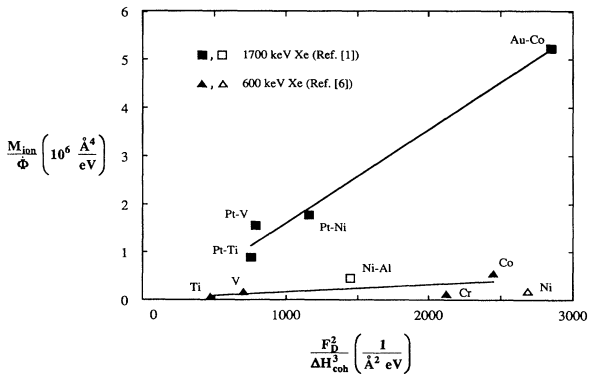

FIG. 4. Experimentally derived values of the normalized mobility $M_{ion}/\dot{\Phi}$, as a function of the parameter, $F_D^2/\Delta H_{coh}^3$ from a thermal-spike analysis of experimental ion-induced grain-growth data from elemental and coevaporated alloy films. Open symbols represent data excluded from least-squares linear fits.

(18). However, the linear fit for the coevaporated data ($r=0.99$) is considerably better than the elemental data ($r=0.68$). The trend is that larger values of $F_D^2/\Delta H_{coh}^3$ result in larger values of normalized mobility. The difference in the slopes of these lines is believed attributable to the different grain-size measurement techniques used as discussed above.

The thermal-spike analysis results may be used to determine the value of the constant β used to scale the activation energy for grain growth within the thermal spike with the cohesive energy [Eq. (15)]. A comparison can then be made with ion-beam mixing, in which a similar thermal-spike approach has been successfully applied to describe variations in ion-beam mixing rates observed among bilayer thin films.[29] The ion-beam mixing model also scales the activation energy for atom migration with the average alloy cohesive energy, $Q=-\beta_{IM}\Delta H_{coh}$, with β_{IM} the scaling constant for ion mixing (IM). The slope, m', determined from the plot of the normalized mobilities, $M_{ion}/\dot{\Phi}$, versus the parameter $F_D^2/\Delta H_{coh}^3$ shown in Fig. 4 can be used to find β for the two sets of data. From Eq. (18), β is expressed as

$$\beta=\left[\frac{k_0\delta^2k^2}{4\pi\kappa_0c_0m'}\right]^{1/3} . \quad (25)$$

Values for the constants in the parentheses may be estimated and are given in Table III. Because of uncertainty of the environment within a thermal spike, average, generic values were chosen for the material constants: δ, Ω, k_0, γ, κ_0, and c_0. The resulting values are $\beta=0.07$ (coevaporated films, Ref. 1) and $\beta=0.15$ (elemental films, Ref. 6). These values are less than or about equal to the constant determined previously for ion-beam mixing experiments, $\beta_{IM}=0.14$.[29] The fact that β is only a factor 1–2 different from β_{IM} is quite remarkable, since the two parameters were obtained from experimental data examining different phenomena (mixing versus grain growth). Furthermore the smaller value of β for the coevaporated data is consistent with the idea that atomic diffusion across grain boundaries is easier, having a lower activation energy, than diffusion within the lattice.

The thermal-spike analysis results from Fig. 4 may be further compared with those predicted by the collisional model of Atwater, Thompson, and Smith[7] Their model identifies two bimolecular processes involving collision-

TABLE III. Values of constants used in thermal-spike analysis. Material constants represent average, generic values applicable to all the targets.

Constant	Value
k_0	3×10^{13} sec^{-1}
δ	5 Å
E_d	25 eV
γ	3×10^{14} eV cm^{-2}
Ω	15 Å^3
c_0	1.3×10^{19} eV K^{-1} cm^{-3}
κ_0	6.3×10^{18} eV cm^{-1} K^{-1} sec^{-1}
k	8.62×10^{-5} eV K^{-1}

induced defects and their subsequent thermal migration across grain boundaries. The first of these, a collision-induced vacant site and subsequent atom migration to the vacant site, may be treated in a straightforward manner to yield an analytical expression for the ion-induced mobility. Assuming a modified Kinchin-Pease expression for defect production per ion, per unit depth of the form $N_d = 0.8(F_D/2E_d)$ the ion-induced mobility is expressed as

$$M_{\text{ion}} = \frac{0.8k_0\delta^2\dot{\Phi}\Omega\tau}{E_d kT} e^{-Q_{\text{vm}}/kT} F_D \ , \tag{26}$$

where E_d is the displacement energy, Q_{vm} is the vacancy migration enthalpy, and τ is the vacancy-interstitial pair lifetime. In contrast to Eq. (18), this expression predicts that the normalized mobility should increase linearly with increasing F_D. Figure 5 shows the normalized mobility as a function of F_D alone for the same experiments as shown in Fig. 4. While a linear dependence does exist for the elemental data, it is notably absent in the coevaporated data. Films in this latter data set were expected to behave collisionally the same (similar F_D and displacement energies) but clearly there are large variations in mobility among them.

The slope m'' from the elemental film data in Fig. 5 may be combined with Eq. (26) to determine the vacancy-interstitial lifetime required to account for the observed ion-induced mobility,

$$\tau = \frac{E_d kTm''}{0.8k_0\delta^2\Omega} e^{Q_{\text{vm}}/kT} \ . \tag{27}$$

This expression is evaluated at $T = 77$ K (temperature at which the experiments in Ref. 6 were performed) using the constants given in Table III. The vacancy migration enthalpy is approximated by $Q_{\text{vm}} = 0.15$ eV, which is in the range of activation energies determined from previous ion-induced grain-growth experiments.[5,7] The resulting value of $\tau = 1.8 \times 10^{28}$ sec is unrealistically larger. This result is consistent with the idea that migration of defects is extremely limited at this temperature as expected. Unlike the thermal-spike model, the model of Atwater, Thompson, and Smith[7] with its required thermally-induced migration of collision-induced defects, cannot account for grain growth in low-temperature experiments.

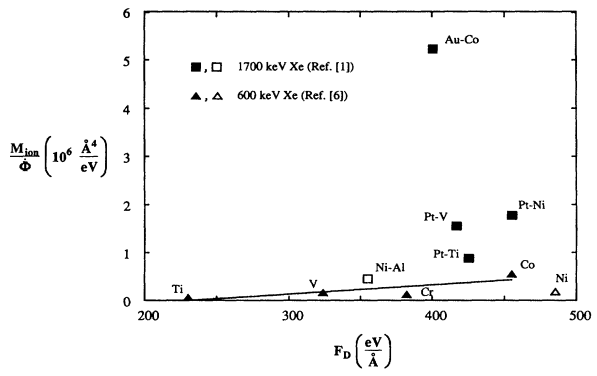

FIG. 5. Experimentally derived values of the normalized mobility $M_{\text{ion}}/\dot{\Phi}$, as a function of the collisional parameter F_D for the same experiments as displayed in Fig. 4. Open symbols represent data excluded from least-squares linear fits.

The above discussion does not unambiguously identify the mechanism of ion-induced grain growth. The thermal-spike description demonstrates consistency with available experimental data that is unmatched by the previously proposed collisional model of Atwater, Thompson, and Smith.[7] However, this comparison of limited data does not exclude the possible existence of a more appropriate collisional description, or some entirely different mechanism, which may account for the linear dependence exhibited by the normalized mobility data from Ref. 6 on F_D (see Fig. 5). It is important to note, though, a possible concern with these samples may be the reactive nature, with respect to oxidation, of most of the films used in the Ref. 6 study. The formation of oxide during film deposition or during irradiation might well be expected to affect the mobility of grain boundaries, through substantial alterations in F_D or cohesive energies. It is further noted that these elements span a variety of crystal structures, suggesting that the grain-growth process may be correlated to structure. In light of such concerns and the limited availability of existing data additional experiments are necessary to elaborate the issue of thermal spike versus other mechanisms of ion-induced grain growth.

Clearly, the thermal-spike model as presented represents a highly idealized picture of how heavy-ion irradiation affects grain growth in single phase systems. However, it does permit an analytical treatment of the grain-growth process in the temperature-independent regime. The model does not take into account the nature of the cascade structure,[30] which may reasonably be expected to vary considerably among different ion/target combinations and in turn lead to varying grain-growth behavior. Also, the model does not account for the weak temperature dependence observed in certain ion-induced grain-growth experiments.[5,7] This and the previous models[7,21] ignore the possible effects presented by the film morphology. The large amounts of surface area present in all the thin-film samples studied represent potential sources and sinks for defects produced during irradiation and may indeed impact on the ion-induced grain-growth process in thin films. In spite of these concerns, the thermal-spike approach does provide a framework in which to incorporate material properties (i.e., ΔH_{coh}) aside from those associated strictly with collisional effects. As demonstrated above, it is thus possible to account for different grain-growth behavior observed in collisionally similar systems.

B. Multilayer films

Experiments investigating ion-induced grain growth have typically been of the type described in the last section. Average grain size is determined from plan view TEM images of a thin-film microstructure as a function of ion dose. Grain boundaries are observed to migrate

substantial distances (hundreds of angstroms) during ion doses extending to 10^{16} cm^{-2}. Such studies have focused on single-phase, elemental films. Systematic studies of grain growth during ion-beam mixing are limited to work performed by Alexander, Was, and Rehn[1] in which grain growth in multilayer and coevaporated alloy films was examined. However, as described below, this experiment or more generally experiments of this type, are inadequate for evaluating the thermal-spike model as developed in Sec. III B.

The details of the experiment performed by Alexander, Was, and Rehn are given in Ref. 1. Briefly, 400-Å thick alloy films were evaporated in multilayer and coevaporated form with an average composition of about $A-20$ at. % B with A = Au, Pt, Ni and B = Co, Ti, V, Ni, and Al. Multilayers consisted of alternating layers of 50–60-Å thick A-element layers and 10–20-Å thick B-element layers. Grain size versus ion dose data was obtained for the films irradiated at room temperature with 1.7 MeV Xe in the HVEM/Tandem facility at Argonne National Laboratory.[31]

The results of this experiment indicated that the heat of mixing (ΔH_{mix}) in the multilayers influenced grain-growth rates relative to rates in the coevaporated films. As described in an earlier section, a thermal-spike model may be used to describe such a phenomenon in which an effect due to the heat of mixing is incorporated via a Darken effect. However, the present experiments were inappropriate for evaluating the modeled heat of mixing effect.

Application of the thermal-spike model required certain assumptions regarding the geometry the thin-film multilayers. In order for the concentration effect to manifest itself during ion-induced grain growth, a consistent orientation relationship must be present between gradients due to boundary curvature and concentration gradients. If gradients due to curvature are randomly oriented then the thermal-spike model indicates that no net effect of concentration gradients on grain growth is expected. The required orientation relationship is satisfied in the work of Ref. 1 by assuming that the boundary curvature was always directed toward the B-rich side in the as-evaporated multilayers. As a result of their small thickness (~ 15 Å) the B layers formed with a smaller grain size than that of the A element layer and therefore the boundary between the two elements is assumed to always be curved inward toward the B element.

However, even with the geometry assumption, these specific experimental results are inappropriate for evaluation of the model. Measured grain-boundary migration rates exceed expected interdiffusion rates effectively nullifying a premise of the model, i.e., a grain boundary migrates in a concentration gradient. Johnson *et al.*[24] and Ma *et al.*[32] determined mixing efficiencies for a number of Xe ion irradiated bilayers including the alloys used in the present study. These efficiencies are used to estimate the extent of intermixing after a dose of $\Delta\Phi = 10^{14}$ cm^{-2} (see Table IV). Also listed in the table, are measured changes in A-B boundary migration distance ΔL after the same dose increment, as determined from the multilayer grain-growth experiments.[1] The results (Table IV) indicate that boundary migration occurs at a much faster rate than intermixing ($\Delta L > [4Dt]^{1/2}$). The A-B grain boundaries are expected to exit the concentration gradient zones quite rapidly, at very low doses. Therefore, the multilayer experiments as performed are not "sensitive" enough to test the particular heat of mixing effect predicted by the thermal-spike grain-growth model developed in Sec. III B.

TABLE IV. Comparison of calculated Xe ion-induced intermixing at an A-B interface and measured average A-B grain-boundary migration distance ΔL after an ion dose of $\Delta\Phi = 10^{14}$ cm^{-2} taken from Ref. 1. Ion mixing efficiencies taken from Refs. 24 and 32.

A-B	Ion mixing efficiency $\frac{4Dt}{\Phi}$ ($\times 10^5$ Å^4)	Calculated intermixing $(4Dt)^{1/2}$ (Å)	Measured A-B boundary migration ΔL (Å)
Pt-Ti	1.28	36	57
Pt-V	0.68	26	62
Ni-Al	0.60	24	46
Pt-Ni	0.45	21	87
Au-Co	0.45	21	110

A more sensitive technique would be to examine boundary migration *in situ* during irradiation in the TEM. Conceivably, such an experiment could involve examining the migration of an isolated boundary separating elemental materials. This could be done at the very early stages of the irradiation (low dose) so that the boundary remained in the concentration gradient and its velocity could then be correlated with the thermal-spike model predictions.

V. CONCLUSIONS

Heavy-ion-induced grain growth in elemental and homogeneous alloy films may be described by a thermal-spike model in which irradiation-induced, cylindrical spikes thermally activate atom jumps resulting in boundary migration. For normal grain growth driven by the reduction in boundary curvature, the model predicts a linear dependence of the ion-induced boundary mobility with the quantity $F_D^2/\Delta H_{\text{coh}}^3$, where F_D is the ion and recoil energy deposited in elastic collisions and ΔH_{coh} is the cohesive energy of the material. Using the thermal-spike approach, it is possible to account for variations in grain growth observed among collisionally similar thin-film systems.

In order to comment on the validity of the model, a comparison was made with existing experimental data. Due to the limited nature of the data, an appropriate evaluation could only be made with two data sets involving elemental and coevaporated alloy films. The results of this comparison demonstrated the consistency of the thermal-spike model. Combining analytical results of the model with the experimental data it was possible to determine the value of the proportionality constant relating the cohesive energy to the activation energy for grain growth. This constant was determined to be $\beta = 0.07$ for

the coevaporated films and $\beta=0.15$ for the elemental films. In the case of the coevaporated films, β is less than or equal to the value previously determined for the thermal-spike treatment of ion-beam mixing ($\beta_{IM}=0.14$), and therefore supportive of the idea that atom migration across grain boundaries is easier than migration within the lattice.

The experimental comparison provided in this work, while demonstrating the consistency of the thermal-spike approach, did not permit unambiguous identification of the ion-induced grain-growth mechanism in single phase films. Clearly, additional experiments are necessary to elaborate this issue.

The thermal-spike approach was also used to describe grain growth in multilayer films by including the added effect of concentration gradients on boundary migration. In addition, the influence of the heat of mixing (ΔH_{mix}) on atomic mobility and boundary migration was incorporated via a Darken effect.

ACKNOWLEDGMENTS

The authors are grateful to a number of individuals for helpful discussions including L. Rehn, J. Liu, H. Atwater, C. Allen, P. Borgesen, and D. Lilienfeld. This work was supported under NSF Grant Nos. DMR8603174 and DMR8903138 and under DOE Contract No. W-31-109-Eng-38.

APPENDIX

The combined effect of grain-boundary curvature and concentration gradients on ion-induced grain growth is determined by evaluating a thermal-spike parameter η_{TOT} as shown in this appendix. The combined effect of the gradients can be described by summing the independent rates for individual atom migration due to each driving force. Referring to Fig. 3, the rate of B-atom jumps from site I to site II, $\nu^B_{I\to II}$ is

$$\nu^B_{I\to II}=k_0 e^{-Q_B/kT} . \tag{A1}$$

Likewise for B-atom jumps in the opposite direction, the rate $\nu^B_{II\to I}$ is

$$\nu^B_{II\to I}=k_0 e^{-(Q_B+\Delta\mu_{curv(B)}+\Delta\mu_{conc(B)})/kT} . \tag{A2}$$

So the net rate of B-atom transfers from site I to site II is $\nu^B_{net}=\nu^B_{I\to II}-\nu^B_{II\to I}$ or,

$$\nu^B_{net}=k_0 e^{-Q_B/kT}(1-e^{-(\Delta\mu_{curv(B)}+\Delta\mu_{conc(B)})/kT}) . \tag{A3}$$

As was done before for the sole driving force of grain-boundary curvature, assuming $(\Delta\mu_{curv(B)}+\Delta\mu_{conc(B)}) \ll kT$, a power-series expansion can be used to approximate the exponential term in the brackets, simplifying Eq. (A3) to

$$\nu^B_{net}=\frac{k_0(\Delta\mu_{curv(B)}+\Delta\mu_{conc(B)})}{kT}e^{-Q_B/kT} . \tag{A4}$$

This is converted to the B-atom jump rate per unit volume, by multiplying by the atomic concentration of B atoms in the alloy expressed as $f_B\rho$,

$$R_B=\frac{k_0 f_B\rho(\Delta\mu_{curv(B)}+\Delta\mu_{conc(B)})}{kT}e^{-Q_B/kT} . \tag{A5}$$

This expression may be described as the individual contributions due to each driving force, such that $R_B=R_{curv(B)}+R_{conc(B)}$ where,

$$R_{curv(B)}=\frac{k_0 f_B\rho\Delta\mu_{curv(B)}}{kT}e^{-Q_B/kT} , \tag{A6a}$$

$$R_{conc(B)}=\frac{k_0 f_B\rho\Delta\mu_{conc(B)}}{kT}e^{-Q_B/kT} . \tag{A6b}$$

Now consider the effects of gradients on A-atom migration. The rate of A-atom jumps from site I to site II, $\nu^A_{I\to II}$ is

$$\nu^A_{I\to II}=k_0 e^{-(Q_A+\Delta\mu_{conc(A)})/kT} . \tag{A7}$$

Likewise, for A-atom jumps in the opposite direction, $\nu^A_{II\to I}$ is

$$\nu^A_{II\to I}=k_0 e^{-(Q_A+\Delta\mu_{curv(A)})/kT} . \tag{A8}$$

The net rate of A-atom transfers from site I to site II is $\nu^A_{net}=\nu^A_{I\to II}-\nu^A_{II\to I}$ or

$$\nu^A_{net}=k_0 e^{-Q_A/kT}(e^{-\Delta\mu_{conc(A)}/kT}-e^{-\Delta\mu_{curv(A)}/kT}) . \tag{A9}$$

For $\Delta\mu_{curv(A)}\ll kT$ and $\Delta\mu_{conc(A)}\ll kT$, then the exponentials in the parentheses may be approximated by power-series expansions, simplifying Eq. (A9) to

$$\nu^A_{net}=\frac{k_0(\Delta\mu_{curv(A)}-\Delta\mu_{conc(A)})}{kT}e^{-Q_A/kT} . \tag{A10}$$

As done previously for B atoms, Eq. (A10) can be used to determine the net rate of A-atom jumps per unit volume as $R_A=R_{curv(A)}-R_{conc(A)}$, where

$$R_{curv(A)}=\frac{k_0 f_A\rho\Delta\mu_{curv(A)}}{kT}e^{-Q_A/kT} , \tag{A11a}$$

$$R_{conc(A)}=\frac{k_0 f_A\rho\Delta\mu_{conc(A)}}{kT}e^{-Q_A/kT} . \tag{A11b}$$

Therefore, the total net transfer rate of atoms per unit volume from site I to site II due to both driving forces is $R_{TOT}=R_A+R_B$, or

$$R_{TOT}=R_{curv(A)}+R_{curv(B)}+R_{conc(B)}-R_{conc(A)} . \tag{A12}$$

As observed in this expression, the total rate is simply a summation of the independent rates in the various directions of the respective gradients.

The expression in Eq. (A12) is used to determine η_{TOT} by substituting the expressions for the individual terms as given by Eqs. (A6a), (A6b), (A11a), and (A11b), and integrating over space and time [Eq. (7)]. Performing the integrations and making the substitutions of $p=1$ and $Q=-\beta\Delta H_{coh}$, the resulting η_{TOT} is found to be

$$\eta_{\mathrm{TOT}}=\frac{k_0\rho k^2F_D^2}{\pi\kappa_0 c_0\beta^2}\left[\frac{\Delta\rho_B}{\rho_B}\frac{f_B}{8\Delta H^2_{\mathrm{coh}(B)}}\left[1+\frac{4}{\beta}\frac{\Delta H_{\mathrm{mix}}}{\Delta H_{\mathrm{coh}(B)}}\right]-\frac{\Delta\rho_A}{\rho_A}\frac{f_A}{8\Delta H^2_{\mathrm{coh}(A)}}\left[1+\frac{4}{\beta}\frac{\Delta H_{\mathrm{mix}}}{\Delta H_{\mathrm{coh}(A)}}\right]-\frac{\gamma\Omega}{\beta L}\left[\frac{f_A}{\Delta H^3_{\mathrm{coh}(A)}}+\frac{f_B}{\Delta H^3_{\mathrm{coh}(B)}}\right]\right]. \tag{A13}$$

This equation may be written as $\eta_{\mathrm{TOT}}=\eta_{\mathrm{conc}}+\eta'$, where the contribution of the concentration gradient terms η_{conc} and the curvature gradient terms η' are separately expressed as

$$\eta_{\mathrm{conc}}=\frac{k_0\rho k^2F_D^2}{\pi\kappa_0 c_0\beta^2}\left[\frac{\Delta\rho_B}{\rho_B}\frac{f_B}{8\Delta H^2_{\mathrm{coh}(B)}}\left[1+\frac{4}{\beta}\frac{\Delta H_{\mathrm{mix}}}{\Delta H_{\mathrm{coh}(B)}}\right]-\frac{\Delta\rho_A}{\rho_A}\frac{f_A}{8\Delta H^2_{\mathrm{coh}(A)}}\left[1+\frac{4}{\beta}\frac{\Delta H_{\mathrm{mix}}}{\Delta H_{\mathrm{coh}(A)}}\right]\right] \tag{A14}$$

$$\eta'=-\frac{k_0\gamma\Omega\rho k^2F_D^2}{\pi\kappa_0 c_0 L\beta^3}\left[\frac{f_A}{\Delta H^3_{\mathrm{coh}(A)}}+\frac{f_B}{\Delta H^3_{\mathrm{coh}(B)}}\right]. \tag{A15}$$

Equation (A15) for η' is a variant of the expression derived previously for the curvature driving force represented by η in Eq. (16). Equation (A15) explicitly accounts for the cohesive energy of the individual atomic components whereas Eq. (16) uses a single averaged value.

[1]D. E. Alexander, G. S. Was, and L. E. Rehn, J. Appl. Phys. **70**, 1252 (1991).

[2]J. Li, J. C. Liu, and J. W. Mayer, Nucl. Instrum. Methods B **36**, 306 (1989).

[3]J. C. Liu and J. W. Mayer, Nucl. Instrum. Methods B **19/20**, 538 (1987).

[4]J. C. Liu, M. Nastassi, and J. W. Mayer, J. Appl. Phys. **62**, 423 (1987).

[5]J. C. Liu, J. Li, and J. W. Mayer, J. Appl. Phys. **67**, 2354 (1990).

[6]P. Borgesen, D. A. Lilienfeld, and H. Massad, in *Surface Chemistry and Beam-Solid Interactions,* edited by H. A. Atwater, F. A. Houle, and D. H. Lowndes, MRS Symposia Proceedings No. 201 (Materials Research Society, Pittsburgh, 1991), pp. 393-398.

[7]H. A. Atwater, C. V. Thompson, and H. I. Smith, J. Appl. Phys. **64**, 2337 (1988).

[8]D. E. Alexander, G. S. Was and L. E. Rehn, in *Beam-Solid Interactions: Physical Phenomena,* edited by J. A. Knapp, P. Borgesen, and R. A. Zuhr, MRS Symposia Proceedings No. 157 (Materials Research Society, Pittsburgh, 1990), pp. 155–160.

[9]J. C. Liu, J. Li, J. W. Mayer, C. W. Allen, and L. E. Rehn, in *Processing and Characterization of Materials Using Ion Beams,* edited by L. E. Rehn, J. Greene, and F. A. Smidt, MRS Symposia Proceedings No. 128 (Materials Research Society, Pittsburgh, PA, 1989), pp. 297-302.

[10]P. Wang, D. A. Thompson, and W. W. Smeltzer, Nucl. Instrum. Methods B **16**, 288 (1986).

[11]P. Wang, D. A. Thompson, and W. W. Smeltzer, Nucl. Instrum. Methods B **7/8**, 97 (1985).

[12]J. C. Liu and J. W. Mayer, in *Fundamentals of Beam-solid Interactions and Transient Thermal Processing,* edited by M. J. Aziz, L. E. Rehn, and B. Stritzker, MRS Symposia Proceedings No. 100 (Materials Research Society, Pittsburgh, 1988), pp. 357–362.

[13]P. V. Pavlov, A. P. Pavlov, and D. I. Tetelbaum, Phys. Status Solidi A **120**, 441 (1990).

[14]B. X. Liu and X. Zhou, Phys. Status Solidi A **124**, K101 (1991).

[15]L. E. Rehn and P. R. Okamoto, Nucl. Instrum. Methods B **39**, 104 (1989).

[16]B. M. Paine and R. S. Averback, Nucl. Instrum. Methods B **7/8**, 666 (1985).

[17]H. Wiedersich, Nucl. Instrum. Methods B **7/8**, 1 (1985).

[18]R. S. Averback and M. A. Kirk, in *Surface Alloying by Ion, Electron, and Laser Beams,* edited by L. E. Rehn, S. T. Picraux, and H. Wiedersich (American Society for Metals, Metals Park, OH, 1987), pp. 91–135.

[19]J. B. Biersack and L. G. Haggmark, Nucl. Instrum. Methods **174**, 257 (1980).

[20]H. A. Atwater, C. V. Thompson, and H. I. Smith, Phys. Rev. Lett. **60**, 112 (1988).

[21]J. C. Liu, Ph.D. thesis, Cornell University, 1989.

[22]G. H. Vineyard, Radiat. Eff. **29**, 245 (1976).

[23]P. G. Shewmon, *Transformations in Metals* (McGraw-Hill, New York, 1969).

[24]W. L. Johnson, Y. T. Cheng, M. Van Rossum, and M-A. Nicolet, Nucl. Instrum. Methods B **7/8**, 657 (1985).

[25]M. Doyama and J. S. Koehler, Acta. Metall. **24**, 871 (1976).

[26]P. G. Shewmon, *Diffusion in Solids* (The Minerals, Metals & Materials Society, Warrendale, PA, 1989).

[27]C. Kittel, *Introduction to Solid State Physics,* 5th ed. (Wiley, New York, 1976), p. 74.

[28]E. A. Grey and G. T. Higgins, Acta. Metall. **21**, 309 (1973).

[29]M. Van Rossum and Y-T. Cheng, in *Ion Implantation 1988,* edited by F. H. Wohlbier (Trans Tech Publications Ltd., Switzerland, 1988), pp. 1–31.

[30]F. Rossi and M. Nastasi, J. Appl. Phys. **69**, 1310 (1991).

[31]C. W. Allen, L. L. Funk, E. A. Ryan, and A. Taylor, Nucl. Instrum. Methods B **40/41**, 553 (1989).

[32]E. Ma, T. W. Workman, W. L. Johnson, and M-A. Nicolet, Appl. Phys. Lett. **54**, 413 (1989).

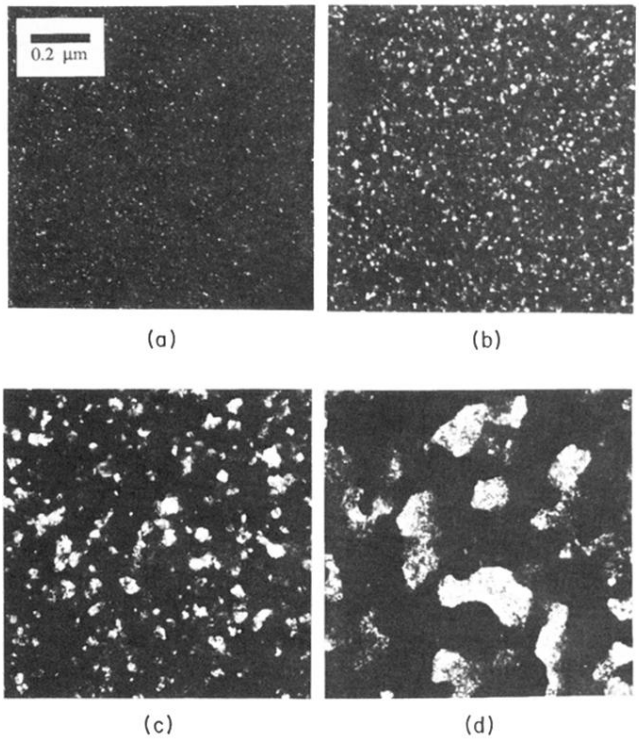

FIG. 1. Example of ion-induced grain growth in Pt-Ti multilayer films irradiated with 1.7 MeV Xe ions at room temperature. (a) As-deposited, (b) 10^{14} cm^{-2}, (c) 10^{15} cm^{-2}, (d) 10^{16} cm^{-2}.